Infrared spectroscopic study on lattice dynamics in $CaFeO_3$

C. X. Zhang,[1] H. L. Xia,[1] H. Liu,[1] Y. M. Dai,[2] B. Xu,[1,3] R. Yang,[1] Z. Y. Qiu,[1] Q. T. Sui,[1]
Y. W. Long,[1,4] S. Meng,[1,4] and X. G. Qiu[1,4,*]

[1]*Beijing National Laboratory for Condensed Matter Physics, Institute of Physics, Chinese Academy of Sciences, P.O. Box 603, Beijing 100190, People's Republic of China*

[2]*Condensed Matter Physics and Materials Science Department, Brookhaven National Laboratory, Upton, New York 11973, USA*

[3]*Center for High Pressure Science and Technology Advanced Research, Beijing 100094, People's Republic of China*

[4]*Collaborative Innovation Center of Quantum Matter, Beijing 100190, People's Republic of China*

(Received 3 December 2016; published 14 February 2017)

The change of the lattice dynamics upon the charge disproportionation (CD) transition has been investigated for the $CaFeO_3$ crystal by measuring its infrared optical spectra. Across the CD transition, $CaFeO_3$ undergoes a metal-insulator transition, and it is found that below $T_{CD} \approx 290$ K the low-frequency optical conductivity gradually decreases to a rather low value and is dominated by a series of infrared-active phonons. Intriguingly, accompanied by the CD transition, two prominent phonon modes at ∼243 and ∼559 cm^{-1}associated with the vibrations of Fe-O bonds show obvious redshift and asymmetric line shapes characterized by a Fano profile, suggesting a strong electron-phonon coupling. This coupling behavior reveals an intimate relationship between charge and lattice in the CD transition of $CaFeO_3$.

DOI: 10.1103/PhysRevB.95.064104

I. INTRODUCTION

Strongly correlated transition metal oxides have been attracting much attention since they are often related to interesting phenomena such as high-temperature superconductivity and colossal magnetoresistance [1]. Among them, perovskites containing iron in the high valence state Fe^{4+} are of great interest, because of their special physical properties such as the metal-insulator transition (MIT), charge ordering, and screw spin structure [2–5]. In this class, $CaFeO_3$ containing Fe^{4+} undergoes a charge-disproportionation (CD) transition ($2Fe^{4+} \rightarrow Fe^{3+} + Fe^{5+}$) and a structural phase transition at $T_{CD} \approx 290$ K which transforms the system from a high temperature metal to a low temperature insulator, and exhibits helimagnetic order at $T_N \sim 120$ K [6]. Such phenomena make $CaFeO_3$ an interesting compound to study the interplay of charge, lattice, and spin degrees of freedom.

After the discovery of the CD transition in $CaFeO_3$ [7], neutron diffraction experiments [6] revealed that Fe-O bond length differentiates below T_{CD}, which corresponds to the structural transition from the room temperature orthorhombic structure to a low temperature monoclinic one. Such a lowering of symmetry due to a structural transition should lead to changes in phonons, just as the cases in $SrTiO_3$ [8] and iron pnictides [9].

Indeed, optical spectroscopy of $CaFeO_3$ has shown changes in phonons upon its CD transition. Raman spectroscopy performed by Ghosh *et al.* [10] finds that a phonon mode at 708 cm^{-1}splits into two modes at T_{CD}, corresponding to the distortion of FeO_6 octahedra. Nuclear resonant x-ray inelastic scattering [11] shows changes in phonon density of states, which implies that the structural change associated with the CD transition is evident and the electron-phonon interaction plays an important role on the CD transition.

Infrared spectroscopy is a powerful tool to study phonons, electron-lattice coupling, and charge or spin ordered states [12–15]. Fujioka *et al.* [16] have performed infrared (IR) optical spectroscopy studies on $CaFeO_3$ and find that electronic spectral weight transforms in a much larger energy region than the gap and suggests that the Hund's coupling plays important roles on the CD transition [17]. However, although the authors also stress the effects of lattice on the CD transition, the IR active phonons have not been studied in detail. An investigation on the lattice vibrations can reveal useful information about the electron-phonon coupling, which often embodies itself as broad polaronic peaks [18] or asymmetric phonon line shapes [19]. Fano line shapes of phonons have been observed in many systems such as cuprates [13], pnictides [9,19], and graphene [20]. Their Fano line shapes are often considered as the results of couplings between the discrete phonon and the continuum of electron-hole excitations or spin excitation. Therefore, studying the temperature dependence of phonon line shapes provides a way to investigate the evolution of electron-phonon interaction upon the CD transition.

In the present work, we investigate the IR-active phonon modes in $CaFeO_3$ from 310 down to 7 K. We observe that several phonon peaks emerge below T_{CD} and T_N and that two phonons at ∼243 and ∼559 cm^{-1}associated with the vibrations of Fe-O bonds show redshift and have asymmetric line shapes below T_{CD}. Such asymmetric line shapes are fitted by Fano functions, and their temperature dependence is studied. Our results reveal that the phonons in $CaFeO_3$ change evidently below T_{CD}, implying the important role of electron-phonon interactions upon the CD transition, which is consistent with the previous investigations performed by Raman spectroscopy [10] and nuclear resonant x-ray inelastic scattering [11].

II. EXPERIMENT

The single crystals of $CaFeO_3$ were obtained by a two-step synthesis method combining the floating-zone technique and high-oxygen-pressure treatment [21]. The temperature

*xgqiu@iphy.ac.cn

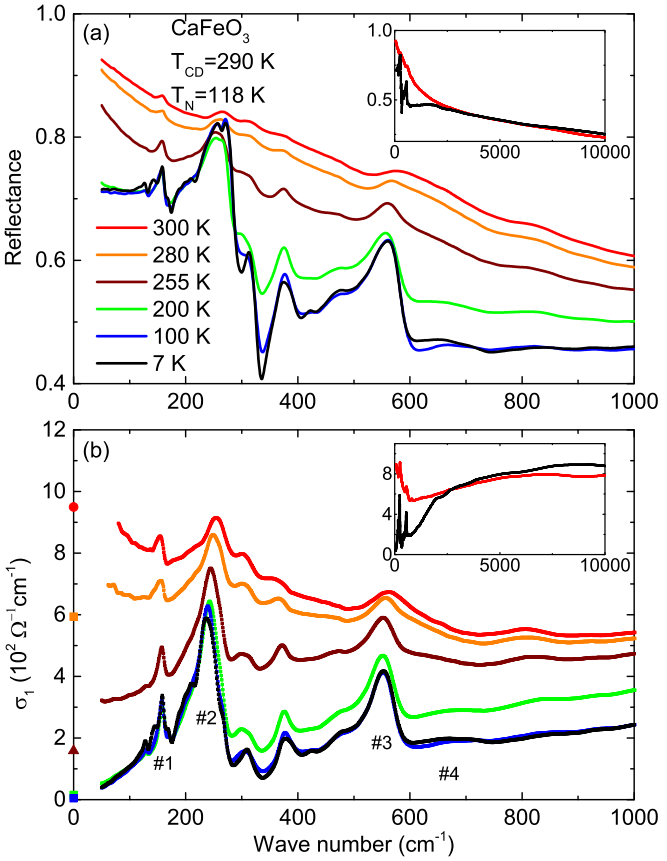

FIG. 1. (a) The reflectivity in the far infrared region for $CaFeO_3$ at several representative temperatures. (b) The low frequency optical conductivity $\sigma_1(\omega)$ for $CaFeO_3$ deduced from the K-K transformation of the reflectivity. The colored symbols on the vertical axis are dc values of conductivity obtained from the measurement of resistivity. The insets in (a) and (b) show the reflectivity and optical conductivity up to 10 000 cm^{-1}, respectively.

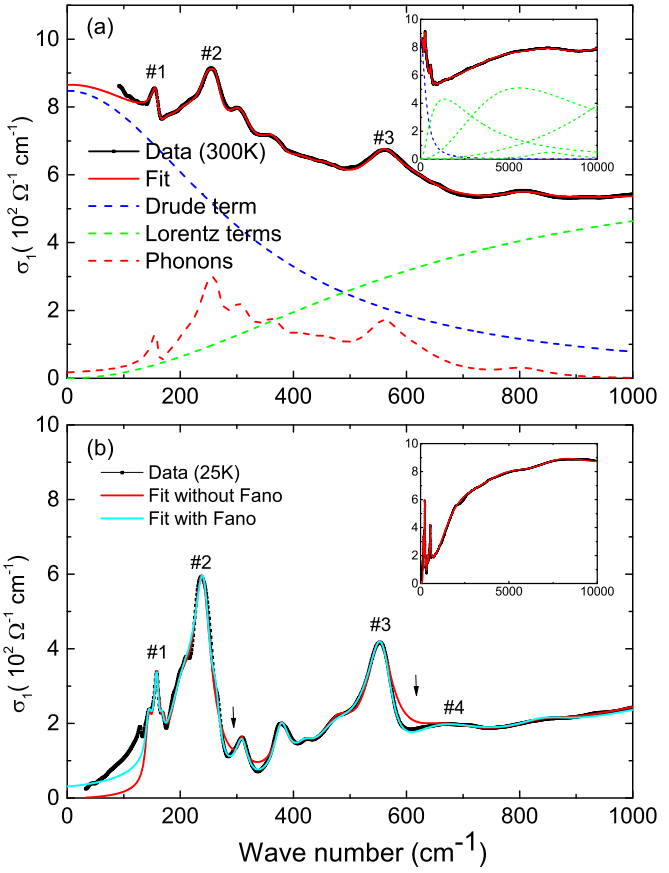

FIG. 2. The fitting curves of the real part of optical conductivity in the far infrared region at (a) $T = 300$ and (b) $T = 25$ K. The phonon modes discussed in the text are labeled by #1 to #4. The arrows in (b) signify the deviation of the Drude-Lorentz fitting. The insets show the spectra up to 10 000 cm^{-1}.

dependence of resistivity and magnetic susceptibility was measured to characterize the T_{CD} and T_N. Both of them ($T_{CD} \approx 290$ and $T_N \approx 118$ K) are very consistent with the results reported by Fujioka *et al.* [16] in single-crystal samples.

The reflectivity $R(\omega)$ was measured at a near-normal angle of incidence on a Fourier transform infrared spectrometer (Bruker 80v). An *in situ* gold overfilling technique [22] was used to obtain the absolute reflectivity of the samples. Data from 60 to 15 000 cm^{-1} were collected at different temperatures ranging from 7 to 310 K. $R(\omega)$ in the visible and UV range was measured up to 40 000 cm^{-1} at room temperature with an AvaSpec-2048 $\times 14$ optical fiber spectrometer.

III. RESULTS

Figure 1(a) shows the far-infrared reflectivity $R(\omega)$ of $CaFeO_3$ at different temperatures. At 300 K, $R(\omega)$ increases toward unity with decreasing photon energy, indicating the metallic nature. When the temperature is decreased below T_{CD} of 290 K, the low-energy $R(\omega)$ is suppressed gradually, showing the transition from a room-temperature metal to a low-temperature insulator. Below 100 K, $R(\omega)$ changes only a little in the far-IR region. These results are consistent with the work of Fujioka *et al.* [16]. The behavior of the CD transition in $CaFeO_3$ is different from the situation in $La_{1/3}Sr_{2/3}FeO_3$. $La_{1/3}Sr_{2/3}FeO_3$ undergoes a charge-ordering transition ($3Fe^{3.67+} \rightarrow 2Fe^{3+} + Fe^{5+}$) at $T_{CO} = 200$ K [23], and its reflectivity $R(\omega)$ decreases abruptly near T_{CO} and does not change much below T_{CO} [24]. In addition, from Fig. 1(a) one finds that sharp phonon peaks become prominent with the decreasing temperature.

In order to obtain the optical conductivity, extrapolation and a Kramers-Kronig transformation of the reflectivity spectra are performed. At low frequency, a constant extrapolation is employed. Above 40 000 cm^{-1}, a constant reflectivity up to 12.5 eV is utilized, followed by a free-electron (ω^{-4}) response. Figure 1(b) shows the real part of the optical conductivity $\sigma_1(\omega)$ in the far-infrared region at different temperatures. As the temperature is lowered from $T_{CD} \approx 290$ K, the optical conductivity in the far-infrared region decreases gradually, reflecting the gap opening. From 200 to 7 K, only small changes of the optical conductivity occur in the low energy region, implying the gap opening process has been saturated around 200 K. This phenomenon is consistent with the trend of its structural transition revealed by neutron scattering [6], which showed that the lattice transformation occurred in the

temperature range between ∼290 and ∼220 K. One may observe that at the low temperature of $T = 7$ K, $\sigma_1(\omega)$ in the low energy region below 1000 $cm^{-1}$is still finite beneath the phonon peaks, which implies the existence of some states in the gap region. Such states might have resulted from the incompleteness of the gap opening, gap nodes due to band anisotropy, or midgap states due to defects or local modes [25]. From Fig. 1(b), one also notices that as the temperature decreases the phonon peaks become more prominent, and that several new peaks emerge below T_{CD}. For later convenience, we label these peaks as follows: 160 (#1), 243 (#2), 559 (#3), and 652 cm^{-1} (#4). Upon decreasing the temperature, the phonons #2 and #3 redshift and show asymmetric line shapes. One also notices that new modes emerge on the two sides of the #1 phonon peak below 100 K, which may be related to the antiferromagnetic phase transition at $T_N \approx 118$ K.

We fitted the optical conductivity spectra $\sigma_1(\omega)$ by the Drude-Lorentz model with the following formula:

$$\sigma_1(\omega) = \frac{2\pi}{Z_0}\left[\frac{\Omega_p^2}{\omega^2\tau + \frac{1}{\tau}} + \sum_{k=1}^{n}\frac{\gamma_k\omega^2\Omega_k^2}{\left(\omega_{0,k}^2 - \omega^2\right)^2 + \gamma_k^2\omega^2}\right], \quad (1)$$

where Z_0 is the vacuum impedance. The first term describes the free-carrier Drude response, characterized by a plasma frequency Ω_p and a scattering rate $1/\tau$. The second term describes a sum of Lorentz oscillators, each having a resonance frequency $\omega_{0,k}$, a line width γ_k and an oscillator strength Ω_k. For illustration, we show the data at $T = 300$ and $T = 25$ K and their fitting curves in Fig. 2. Except for some phonon peaks in the far-IR region, the Drude-Lorentz model well fits the data. As the temperature is lowered from 290 K, the Drude component shrinks gradually, and the Drude component is unnecessary to fit the data below 200 K.

From Fig. 2(b), one notices that the phonon peaks #2 and #3 (labeled by arrows) can not be fit well by the Drude-Lorentz model, because of their asymmetric line shapes. Such asymmetric line shape can be fit by a Fano function as what has been done in Ref. [15]. Fano functions have the form as follows [13–15]:

$$\sigma_1(\omega) = \frac{2\pi}{Z_0}\frac{\Omega_F^2}{\gamma_F}\frac{q^2 + 4q\epsilon - 1}{q^2(1 + 4\epsilon^2)}, \quad (2)$$

where $\epsilon = (\omega - \omega_F)/\gamma_F$, ω_F is the resonance frequency, γ_F the line width, and Ω_F the strength. The asymmetry of the Fano line shape is described by a dimensionless parameter q. In general, the Fano line shape of a phonon mode is considered as the result of the coupling of phonon with a continuum of charge or spin excitations [12–15]. To make a consistent analysis, we fit the phonon peaks #2 and #3 by Fano functions in the whole temperature range. The temperature dependence of the peak positions and Fano factors of corresponding modes in $CaFeO_3$ (#2 and #3) is shown in Fig. 3.

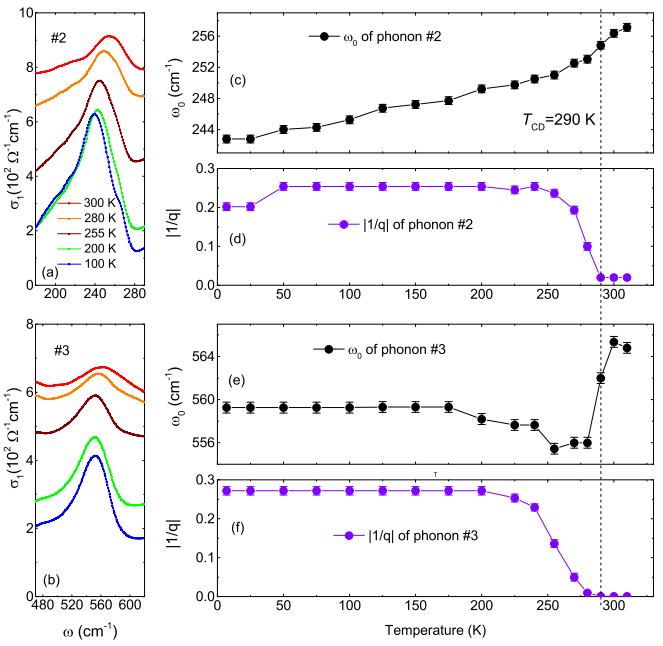

FIG. 3. (a),(b) Line shapes of the phonons #2 and #3. (c)–(f) The resonance frequencies ω_0 and the Fano parameters $|1/q|$ of the #2 and #3 phonon modes determined from the fittings at various temperatures.

IV. DISCUSSION

To have a qualitative understanding of the phonons in $CaFeO_3$, it might be helpful to compare the spectra in Fig. 1(b) with those of $SrFeO_3$ [26] and $R_{1/3}Sr_{2/3}FeO_3$ (R = La,Pr,Nd,Sm,Gd) [27]. Taking $La_{1/3}Sr_{2/3}FeO_3$, for example, the main structures in Fig. 1(b) are similar to Fig. 3 in the paper of Ishikawa *et al.* [24]. Three sharp-peak structures in $La_{1/3}Sr_{2/3}FeO_3$ correspond to the optical phonon modes of the external mode (∼160), the bending mode (∼260), and the stretching mode (∼560 cm^{-1}). In the present case of $CaFeO_3$, the three corresponding modes are found in Fig. 2(b) at 160 (#1), 243 (#2), and 559 cm^{-1} (#3), respectively. From Fig. 3 in the paper of Ishikawa *et al.* [24], one finds the splitting and shifting of the bending mode and the stretching mode below T_{CO}. According to Park *et al.* [27], the shifting and/or splitting of the bending mode and the stretching mode is the result of lattice distortions accompanied by the charge ordering transition.

In order to make a better understanding of these phonon modes, *ab initio* calculations are performed with the Vienna *ab initio* simulation package (VASP). To treat the localized Fe-*d* electrons and the exchange and correlation interactions, the PBE+U approximation [28] is applied to $CaFeO_3$ with the on-site Coulomb parameters $U = 5.3$ eV. The calculation model is relaxed until the force on each atom is less than 0.01eV/Å. As an orthorhombic crystal, $CaFeO_3$ has a $GdFeO_3$ structure at room temperature belonging to the space group *Pbnm* [29]. Accordingly, it has 24 Raman-active phonons [10], 33 IR-active optical phonons, and 3 acoustic phonons. The IR-active optical phonons are given by irreducible representations as $8A_u + 7B_{1u} + 9B_{2u} + 9B_{3u}$. The calculated phonon frequencies are listed in Table I and the vibration patterns with the frequencies close to the experimental results are shown in Fig. 4.

The redshift of a phonon is often explained by the lattice deformation and change of bond length [9]. For our case of $CaFeO_3$, the Fe-O bond length changes below 290 K: the Fe-O bonds expand and contract alternatively with $\Delta l/l \sim \pm 1\%$

TABLE I. Comparison of the calculated and experimental IR-active phonon modes (in cm^{-1}) at 300 K.

Pbnm symmetry	Calculation	Experiment
A_u	130.9	
B_{1u}	161.2	160
B_{3u}	170.4	
B_{2u}	171.7	
A_u	180.0	
B_{1u}	203.0	
B_{3u}	214.6	
A_u	218.0	
B_{2u}	219.4	
B_{2u}	256.3	256
A_u	257.4	
B_{3u}	265.4	
B_{2u}	273.4	
B_{3u}	281.6	
B_{1u}	291.0	
B_{1u}	303.8	306
A_u	308.1	
B_{3u}	313.9	
B_{2u}	315.1	
B_{2u}	339.5	
B_{3u}	366.9	370
B_{1u}	381.4	
A_u	382.6	
B_{3u}	387.2	
B_{3u}	406.4	
B_{2u}	417.7	
B_{2u}	462.7	
B_{1u}	576.9	
A_u	577.6	565
A_u	587.3	
B_{2u}	590.8	
B_{1u}	604.5	
B_{3u}	604.9	

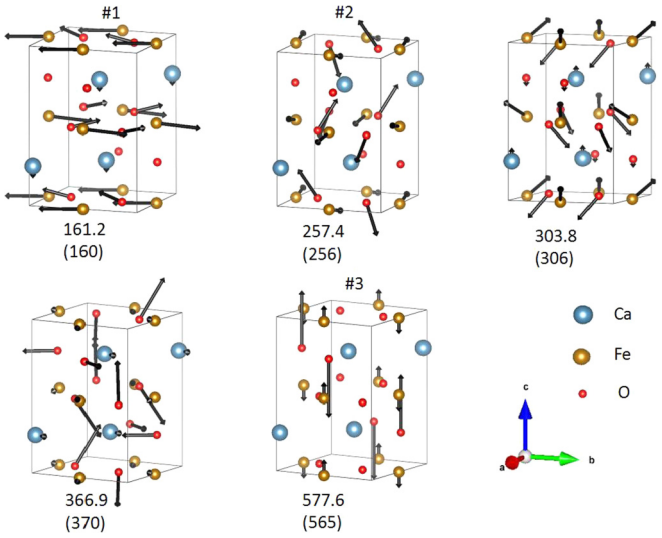

FIG. 4. Vibration patterns of optical phonon modes assigned to the peaks in $\sigma(\omega)$ of $CaFeO_3$ at 300 K. The calculated normal frequencies in cm^{-1} are compared with the observed values at 300 K (in parenthesis).

from 290 to 220 K [6,23]. This kind of bond change alone leads to phonon blueshift; therefore it can not explain redshift of phonons in $CaFeO_3$. However, one notices that $CaFeO_3$ undergoes a CD transition $2Fe^{4+} \rightarrow Fe^{3+} + Fe^{5+}$ at 290 K. Considering the oscillation of the Fe-Fe relative motion, according to the force constant $k \propto Q_1 Q_2 / l^3$, [30] with Q_1 and Q_2 the charges of the ions, $k'/k = 15/16$ leads to a 3 to 4% decreasing of the oscillation frequency, which can explain the 2 to 3% softening of these two phonons at 243 and 559 cm^{-1}. Moreover, the CD transition also changes the numerator $Q_1 Q_2$ of the force constant between the Fe and O atoms from $+4 \times (-2)$ to $+3 \times (-2)$ and $+5 \times (-2)$, with the average unchanged. Such a change does not affect the phonon frequencies at the Γ point of the Brillouin zone. Therefore the overall effect of the valence change of the Fe atoms is softening for the phonons #2 and #3. The external mode is not affected by the CD transition, because it mainly evolves the relative displacement of Ca atoms with respect to FeO_6 octahedra [31] and is less sensitive to the CD and the lattice distortions [24].

In the above, we have mentioned the asymmetric line shapes of #2 and #3 phonon peaks which can not be fit well by Lorentz functions. We fit the spectrum using Fano functions with the parameter $q < 0$ characterizing the asymmetry. The parameter $1/q$, determined from the fittings, is shown in Figs. 3(d) and 3(f) as the function of temperature. From Figs. 3(a) and 3(b) one may observe that the line shapes of these two modes become more symmetric at higher temperatures. As mentioned above, the origin of the asymmetric line shape of a phonon mode is often explained by the coupling between the phonon and electrons or spins. Therefore, the change of the Fano factors of phonons #2 and #3 may imply the change of the electron-phonon coupling. One notices that a gap opens gradually below T_{CD} which changes the electronic density of states (DOS). Therefore, at a low temperature far below T_{CD} the effective electronic states coupling with the phonons are in the higher energy side of these phonons, so the Fano factor $1/q$ will fall in the region $-1 < 1/q < 0$. As temperature increases, electronic states fill the low energy region; then both sides of the phonon mode have electronic states to couple with. Therefore, the line shape of the phonon peak becomes less asymmetric which corresponds to the decrease of $|1/q|$ with the increasing temperature as shown in Figs. 3(d) and 3(f).

It also explains the difference between the two phonons in Figs. 3(d) and 3(f). As the temperature decreases, the 243 cm^{-1} phonon (#2) becomes asymmetric at first, and then the 559 cm^{-1} phonon (#3) follows its trend and begins to become asymmetric at a relatively lower temperature. In order to make it more clear, we take $T = 270$ K, for example. At this temperature, the opened gap is relatively small compared with 559 cm^{-1}; therefore it has little effects on phonon #3. As for the 243 cm^{-1} phonon, its line shape changes at this temperature into an asymmetric form which may imply that the opened gap has affected the electronic DOS around 243 cm^{-1} making the DOS of the two sides of the phonon #2 asymmetric.

Besides peak shift of the bending and stretching mode, a new mode around 650 cm^{-1} (#4) emerges below T_{CD}, which can be seen from Fig. 1(b). The emergence of such a peak is also seen in $R_{1/3}Sr_{2/3}FeO_3$ (R = La,Pr,Nd) [27] and is considered due to the folding of branches of the Fe-O

stretching mode by the periodic charge modulation or associated lattice distortion. In $R_{1/3}Sr_{2/3}FeO_3$ (R = La,Pr,Nd), the strength of the peak increases steeply across T_{CO}. Such a discontinuous increase indicates that the charge-ordering transition is first-order for R = La,Pr,Nd [27]. On the contrary, in our case of $CaFeO_3$, the mode #4 emerges gradually when the temperature lowers from T_{CD}, which is consistent with the second-order property of the CD transition [32].

In summary, the IR-active phonons in $CaFeO_3$ are investigated and the emphasis is placed on phonon evolution upon the CD transition. Additional phonon modes are activated by the CD transition as well as the helimagnetic transition. The redshift and the asymmetric line shapes of the two phonons at 243 and 559 cm^{-1} are analyzed by fitting the data using Fano functions. The central frequencies of these two phonons decrease as the temperature is lowered from T_{CD}. The Fano factors change obviously below T_{CD}, reflecting changes of the electron-phonon coupling and the electronic DOS. It also implies the important role of electron-phonon coupling upon the CD transition.

ACKNOWLEDGMENTS

This work was supported by the MOST of China (973 Projects No. 2015CB921303, No. 2015CB921102, and No. 2014CB921500) and NSFC (Grants No. 91421304, No. 11374345, and No. 11574378).

[1] M. Imada, A. Fujimori, and Y. Tokura, Rev. Mod. Phys. **70**, 1039 (1998).
[2] S. Kawasaki, M. Takano, R. Kanno, T. Takeda, and A. Fujimori, J. Phys. Soc. Jpn. **67**, 1529 (1998).
[3] J. Q. Li, Y. Matsui, S. K. Park, and Y. Tokura, Phys. Rev. Lett. **79**, 297 (1997).
[4] T. Kawakami, S. Nasu, T. Sasaki, K. Kuzushita, S. Morimoto, S. Endo, T. Yamada, S. Kawasaki, and M. Takano, Phys. Rev. Lett. **88**, 037602 (2002).
[5] T. Takeda, Y. Yamaguchi, and H. Watanabe, J. Phys. Soc. Jpn. **33**, 967 (1972).
[6] T. Takeda, R. Kanno, Y. Kawamoto, M. Takano, S. Kawasaki, T. Kamiyama, and F. Izumi, Solid State Sci. **2**, 673 (2000).
[7] M. Takano, N. Nakanishi, Y. Takeda, S. Naka, and T. Takada, Mater. Res. Bull. **12**, 923 (1977).
[8] C. Z. Bi, J. Y. Ma, J. Yan, X. Fang, B. R. Zhao, D. Z. Yao, and X. G. Qiu, J. Phys.: Condens. Matter **18**, 2553 (2006).
[9] B. Xu, Y. M. Dai, B. Shen, H. Xiao, Z. R. Ye, A. Forget, D. Colson, D. L. Feng, H. H. Wen, C. C. Homes, X. G. Qiu, and R. P. S. M. Lobo, Phys. Rev. B **91**, 104510 (2015).
[10] S. Ghosh, N. Kamaraju, M. Seto, A. Fujimori, Y. Takeda, S. Ishiwata, S. Kawasaki, M. Azuma, M. Takano, and A. K. Sood, Phys. Rev. B **71**, 245110 (2005).
[11] J. Matsuno, M. Seto, S. Kitao, Y. Kobayashi, R. Haruki, T. Mitsui, A. Fujimori, and M. Takano, J. Phys. Soc. Jpn. **73**, 2768 (2004).
[12] K.-Y. Choi, Y. G. Pashkevich, K. V. Lamonova, H. Kageyama, Y. Ueda, and P. Lemmens, Phys. Rev. B **68**, 104418 (2003).
[13] W. J. Padilla, M. Dumm, S. Komiya, Y. Ando, and D. N. Basov, Phys. Rev. B **72**, 205101 (2005).
[14] A. B. Kuzmenko, L. Benfatto, E. Cappelluti, I. Crassee, D. van der Marel, P. Blake, K. S. Novoselov, and A. K. Geim, Phys. Rev. Lett. **103**, 116804 (2009).
[15] B. Xu, Y. Dai, J. Han, K. Wang, R. Yang, Y. Yang, W. Zhang, H. Xiao, and X. Qiu, Phys. C: Superconductivity **503**, 25 (2014).
[16] J. Fujioka, S. Ishiwata, Y. Kaneko, Y. Taguchi, and Y. Tokura, Phys. Rev. B **85**, 155141 (2012).
[17] I. I. Mazin, D. I. Khomskii, R. Lengsdorf, J. A. Alonso, W. G. Marshall, R. M. Ibberson, A. Podlesnyak, M. J. Martínez-Lope, and M. M. Abd-Elmeguid, Phys. Rev. Lett. **98**, 176406 (2007).
[18] J. L. M. van Mechelen, D. van der Marel, C. Grimaldi, A. B. Kuzmenko, N. P. Armitage, N. Reyren, H. Hagemann, and I. I. Mazin, Phys. Rev. Lett. **100**, 226403 (2008).
[19] C. C. Homes, Y. M. Dai, J. Schneeloch, R. D. Zhong, and G. D. Gu, Phys. Rev. B **93**, 125135 (2016).
[20] Z. Q. Li, C. H. Lui, E. Cappelluti, L. Benfatto, K. F. Mak, G. L. Carr, J. Shan, and T. F. Heinz, Phys. Rev. Lett. **108**, 156801 (2012).
[21] Y. Long, Y. Kaneko, S. Ishiwata, Y. Taguchi, and Y. Tokura, J. Phys.: Condens. Matter **23**, 245601 (2011).
[22] C. C. Homes, M. Reedyk, D. A. Cradles, and T. Timusk, Appl. Opt. **32**, 2976 (1993).
[23] J. Matsuno, T. Mizokawa, A. Fujimori, Y. Takeda, S. Kawasaki, and M. Takano, Phys. Rev. B **66**, 193103 (2002).
[24] T. Ishikawa, S. K. Park, T. Katsufuji, T. Arima, and Y. Tokura, Phys. Rev. B **58**, R13326(R) (1998).
[25] P. Calvani, M. Capizzi, S. Lupi, P. Maselli, A. Paolone, and P. Roy, Phys. Rev. B **53**, 2756 (1996).
[26] P. Adler, A. Lebon, V. Damljanovic, C. Ulrich, C. Bernhard, A. V. Boris, A. Maljuk, C. T. Lin, and B. Keimer, Phys. Rev. B **73**, 094451 (2006).
[27] S. K. Park, T. Ishikawa, Y. Tokura, J. Q. Li, and Y. Matsui, Phys. Rev. B **60**, 10788 (1999).
[28] J. P. Perdew, K. Burke, and M. Ernzerhof, Phys. Rev. Lett. **77**, 3865 (1996)
[29] V. E. Alexandrov, E. A. Kotomin, J. Maier, and R. A. Evarestov, J. Chem. Phys. **129**, 214704 (2008).
[30] A. de Andrés, S. Taboada, J. L. Martínez, A. Salinas, J. Hernández, and R. Sáez-Puche, Phys. Rev. B **47**, 14898 (1993).
[31] S. Tajima, A. Masaki, S. Uchida, T. Matsuura, K. Fueki, and S. Sugai, J. Phys. C: Solid State Phys. **20**, 3469 (1987).
[32] M. Takano, S. Nasu, T. Abe, K. Yamamoto, S. Endo, Y. Takeda, and J. B. Goodenough, Phys. Rev. Lett. **67**, 3267 (1991).